3rd World Conference on Sustainability, Energy and Environment

Berlin, Germany 08 Dec - 09 Dec 2023

Study of Flared gas Utilization Scenarios through a Small Level Flared gas - Fuel SOFC System

Mariem Hentati[1,2], Ahlem Boussetta[1,2], Dhekra Yakoubi[1,2], Amal Elleuch[1,2*], Kamel Halouani[1,2]

[1]Laboratory of Systems Integration and Emerging Energies (LR21ES14), National Engineering School of Sfax (ENIS), University of Sfax, IPEIS, Road Menzel Chaker km 0.5, P.O. Box 1172, Sfax 3018, Tunisia

[2]Smart Bio-Energy Systems, Digital Research Center of Sfax, Technopole of Sfax, Sakiet Ezzit, P.O. Box 275, Sfax 3021, Tunisia

Abstract.

The oil and gas sector produces a substantial volume of emissions, mainly generated from flaring, which adds to the total energy loss in oil and gas plants and significantly influences air quality. Faced with this challenge, several options have been developed for flared gas recovery. Among these solutions, the solid oxide fuel cell (SOFC) system is a new approach that was proposed in this study. A numerical model combining kinetic and electrochemical studies was developed. Using ASPEN PLUS, the chemical process under adiabatic conditions in the reactors was simulated to provide a detailed thermodynamic and parametric analysis of the SOFC's functioning. Then, MATLAB software was used to evaluate the electrochemical losses and electrical performance of the SOFC model. As part of this investigation, three internal reforming scenarios (dry reforming (DR), steam reforming (SR) and partial oxidation (PO)) were compared, focusing on their impact on the reformed gas composition at the anodic reaction zone and the SOFC performance. We started by supposing that just CH_4 is feeding the SOFC system. Then the adjustment of SOFC performance was elaborated when real flared gas composition (81% of CH_4) was used. Simulation results favor the SR scenario as the best method for supplying methane to the SOFC anode. The maximum power reached is in the order of 2725 $W.m^{-2}$ using a surface area of 0.00163 m^{-2}. Through this analysis, there is no pre-treatment, and the sweetened flared gas was fed directly to the anode's side of the SOFC.

Keywords: Small Level SOFC System, Internal Methane Reforming, Modeling, Flared gas

1. Introduction

The growing reliance of the human race on energy resources is a foreseeable phenomenon closely linked to the rampant demographic expansion and the heightened competition within the global marketplace. It is important to recognize that a projected increase of about 29.1% in worldwide fossil fuel consumption is predictable from 2009 to 2035 (Aydin, 2015). Nevertheless, despite their longstanding role as a cornerstone of global energy production, fossil fuels now present substantial social and environmental drawbacks. Consequently, in the face of the urgent 21st century challenge, namely climate change, humanity is compelled to intensify its quest for environmentally viable energy sources, to reconsider energy paradigms, and to promote sustainable alternatives.

Although natural gas is preferred as an energy source over oil (Kapsalyamova & Paltsev, 2020), it's important to note that both production processes involve flaring and gas venting operations, which remain inevitable. During natural gas and petrol production, several pollutants, including carbon monoxide (CO), carbon dioxide (CO_2), methane (CH_4), hydrocarbons, unconverted non-methane volatile organic compounds (NMVOC) such as acid gases, and black carbon, are emitted into the environment (Böttcher et al., 2021 ; Shahab-Deljoo et al., 2023). This practice is commonly referred to as gas flaring. Often, natural gas and oil producers choose to flare up the by-product natural gas due to a range of issues, from market and economic constraints to a lack of appropriate regulation and political will. Several reasons can be found in the literature (Loe & Ladehaug, 2012). Three main reasons have been identified for flaring in the literature, one of which is related to safety because handling oil and gas involves dealing with significantly high and fluctuating pressure levels. During the extraction of crude oil, a significant or sudden increase in pressure can potentially trigger explosions. Although such industrial accidents are rare, their effects are destructive and long-lasting, making it very difficult to manage this type of fire (Loe & Ladehaug, 2012). In other words, when pressure in oil or gas facilities becomes excessive or unstable, flaring allows operators to burn the excess gas to prevent pressure-related issues, while safely disposing of the gas in a controlled manner (Loe & Ladehaug, 2012). In addition, several economic and technical reasons can compel operators to resort to flaring. In many cases, gas and oil deposits are located in remote and inaccessible areas, which can result in fluctuations in associated gas production. This situation can make the transportation of associated gas to processing facilities complex and costly. Furthermore, when oil production sites are dispersed over vast geographical areas, capturing and utilizing associated gas is often seen as prohibitively expensive. In such cases, associated gas is typically flared (Loe & Ladehaug, 2012). In other cases where the handling of associated gas is technically and economically feasible, the laws

and regulations of a country can make it difficult or even prohibit companies from marketing the associated gas (Loe & Ladehaug, 2012).

The main challenge to reduce flaring is to select one of the known flared gas recovery (FGR) technologies from several options. Therefore, several research studies and assessments of (FGR) technologies have been studied in the literature. Recent studies show that the electricity generation is only way becoming viable and practical (Khalili-Garakani et al., 2022 ; Khalili-Garakani et al., 2021 ; Tahmasebzadehbaie & Sayyaadi, 2023).

There are two approaches to generating electricity from flared gas, including gas turbines and solid oxide fuel cells (SOFC). The produced electricity could be used on site or sold to the local grid. SOFC power plants are a proven clean-tech alternative for electric utility power generation in residential, commercial and industrial applications. SOFCs lend themselves well to stationary power also to heavy-duty transportation. SOFCs are also able to process a wide variety of hydrocarbons due to their high temperature, which sets them apart favorably from other methods, and they are known for their high electrical efficiency, which can reach up to 65%. When hydrocarbons (C_nH_m) are used as fuel, the hydrocarbon reforming reaction ($C_nH_m + nH_2O \rightarrow (n + 0.5m)H_2 + nCO$) producing H_2 is possible. Moreover, due to the continuous consumption of H_2 by the SOFC electrochemical reaction, the equilibrium conditions of both steam reforming and water-gas conversion reactions shift to the right, which consequently leads to an improvement in hydrocarbon conversion. In another way, SOFCs are able to electrochemically oxidize both H_2 and CO, which are products of reformed hydrocarbons (Elleuch & Halouani, 2020 ; Höber et al., 2023). Therefore, by using a suitable catalyst on the anode side, there is no need for an external reformer system, which subsequently simplifies the overall system design and finally reduces the cost of these power systems (Höber et al., 2023 ; Kang et al., 2009). Additionally, internal reforming is expected to increase SOFC system efficiency by eliminating the energy penalty associated with heat transfer for reforming within an external reformer. So, from a technical and economic point of view, the SOFC system can be one of the best conversion systems to recover flared gas in order to reduce GHGs (Nezhadfard & Khalili-Garakani, 2020 ; Saidi et al., 2014). Natural gas and flared gas, which contain mainly CH_4, i.e., 80 to 95%, are among the interesting fuels for SOFCs, demonstrating a promising performance if compared to the conventional pure H_2 fuel (Dicks et al., 2000 ; Saidi et al., 2014).

In this study, we will carry out a numerical study of SOFC system performance fed by flared gas. The model is a combination of a kinetic and an electrochemical model. The kinetic model was carried out using ASPEN PLUS software, whereas the electrochemical model was developed using MATLAB software.

In the kinetic model, different scenarios that can take place in-situ at the SOFC anode after a variation of the anodic gas feed type, i.e., partial oxidation (PO), steam reforming (SR) and dry reforming (DR), will be compared in terms of their impact on the reformed gas composition recuperated at the anodic reaction zone. These simulation results will serve as input parameters for the electrochemical model developed in order to evaluate the fuel cell polarizations and electrical output. The final objective of this study is to select the optimum way for electricity production using flared gas as fuel for SOFC systems.

2. Numerical methodology

2.1. Kinetic model of the Small level SOFC system

Flared gas, which contains mainly methane (CH_4), i.e., 80-95%, is the most interesting fuel for SOFC. Due to its high methane concentration and the well-developed kinetic models of methane reforming found in the literature. This part starts with supposing that just CH_4 is feeding the SOFC system (Fig.1). Three different reforming scenarios of CH_4 are investigated, including the PO, the SR and the DR. Then, the composition of the feedstock is altered, replacing the initial 100% CH_4 with the composition of flared gas (81.94% of CH_4) taken from a Tunisian processing plant (Tab.1).

Figure 1: SOFC single cell configuration

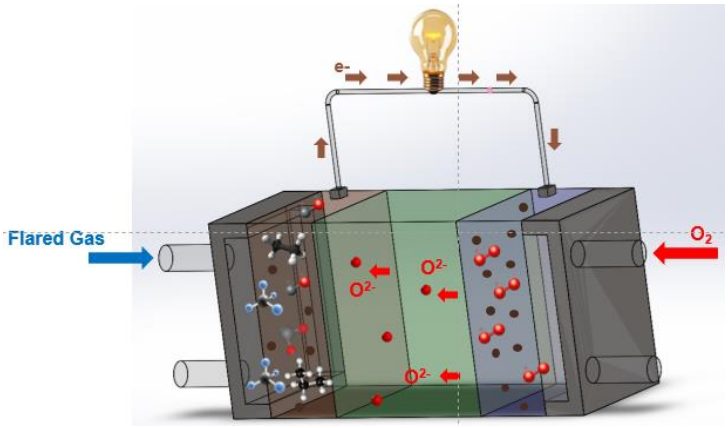

Table 1: Composition of flared gas used in the study

Component	Chemical Formula	Vol.%
Methane	CH_4	0.8194
Carbone dioxide	CO_2	0.0072
Nitrogen	N_2	0.0129
Ethane	C_2H_6	0.0776
Propane	C_3H_8	0.0566
i-butane	C_4H_{10}	0.0061
n-butane	C_4H_{10}	0.0149
i-Pentane	C_5H_{12}-1	0.0024
n-Pentane	C_5H_{12}-2	0.0019
22-MPropane	C_5H_{12}-3	0.0001
Benzene	C_6H_6	0.0009

Small level flared gas-fuel SOFC system based on the internal reforming of flared gas is modeled using ASPEN PLUS software. The Peng-Robinson equation serves as the fundamental method for calculating the physical properties of the system components (Fig.1).

Throughout the simulation, modules essential to the SOFC system's operation are chosen from ASPEN PLUS's library of modules. Calculation formulas relevant to these modules are integrated into process options, utilizing the Fortran language. After the simulation run, the outcome summary conveniently provides direct access to the physical parameters and computed results, such as temperature T, pressure P, mass/molar flowrate and gas composition. Fig. 2 shows a structural schematic layout of the small level flared gas-fuel SOFC system. It consists of a reformer module, an SOFC module characterized by separate anode and cathode, a heat exchanger, a burner and other parts. The small level flared gas-fuel SOFC system uses a surface area of about 0.00163 m².

Figure 2: The small level flared gas - fuel SOFC system layout modelled with Aspen Plus; Solid lines represent material streams and dotted lines represent energy streams.

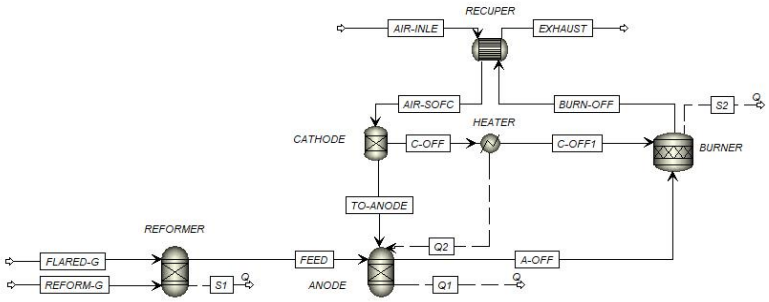

For the reformer module, a Gibbs reactor equilibrium, named "REFORMER," is employed to simulate the reforming reactions occurring inside the anode. The molar flow rate of the fresh flared gas fuel and that of the reforming gas is given in Tab.2.

Table 2: Thermal parameters of the small level flared gas- fuel SOFC system model

Molar flow rate	
Flared gas (Kmol.h^{-1})	0.001201392
Reformed Gas (Kmol.h^{-1})	0.039456
Pure oxygen (TO-ANODE) (Kmol.h^{-1})	0.001436144
Operational Parameters	
Pressure (Bar)	1.035
Fuel utilization in the anode unit (-)	0.86

Knowing that three reforming scenarios are modeled in the framework of this paper. The reforming gas type is taken as air (79% N_2 and 21% O_2) during the PO modeling, H_2O during the SR modeling, and CO_2 during the DR modeling. The same molar flowrate for the reforming gases in the three scenarios (PO, SR and DR) is adopted (Tab.2).
The ratio between these two flows is determined by a specified lambda coefficient (λ), which aligns with the reformer's operational needs. The value of this coefficient is performed to achieve the target oxygen-to-carbon (O/C) ratio using the ASPEN PLUS Calculator C-1 function. The desired O/C ratio is set at 0.61 for the PO and DR scenarios. Nevertheless, the same target hydrogen-to-carbon (H/C) ratio is taken in case of SR scenario. The flared gas is converted inside the adiabatic reformer to produce a stream rich in hydrogen to conduct the electrochemical reactions of the SOFC. The chemical reactions specified in the reformer module are listed in Tab.3 according to the different scenarios.

Table 3: Chemical reactions of the Reformer block fed by flared gas according to the modelled scenarios

Reaction		Reaction name	ΔrH_{287}
Partial Oxidation scenario (PO)			
R1	CH_4+ ½ O2 →CO+2H_2	Partial Oxidation	-36 kJ.mol^{-1}
R2	CH_4+ 2O_2 →CO_2+2H_2O	Complete methane combustion	-802.5 kJ.mol^{-1}
R3	2H_2+ O_2 →2H_2O	Hydrogen combustion	-572 kJ.mol^{-1}
R4	2CO+ O_2 →2CO_2	carbon monoxide oxidation	-561 kJ.mol^{-1}
Steam Reforming scenario (SR)			
R5	CH_4 + H_2O →CO + 3H_2	Steam Reforming	+206 kJ.mol^{-1}
R6	2H_2+ O_2 →2H_2O	Hydrogen combustion	-572 kJ.mol^{-1}
Dry Reforming scenario (DR)			
R7	CH_4 + CO_2 →2CO +2H_2	Dry Reforming	+247 kJ.mol^{-1}

The stream exiting the reformer module, labeled 'FEED', has its temperature and gas composition automatically calculated by ASPEN PLUS software. This stream is directed to the anode side of the SOFC module. Simultaneously, a separate air stream, designated as “AIR-INLE” delivered to the system at about 20°C, and it is subsequently preheated by introducing it into a recuperator module before reaching the cathode part of the SOFC module.
In order to simulate the heating process, a heat exchanger module type HeatX is chosen and designated as "RECUPER" in our case. The "RECUPER" allows the recovery of heat from the hot exhaust gases called “BURN-OFF” issued from the burner module “BURNER”. These modules ensure the satisfaction of the thermal energy demand of the small level SOFC system by preheating the air sent to the cathode unit. The "CATHODE" unit is designed to function as a variable oxygen separator. So, a SPLITER separator is chosen. It enables effectively divides the input flow "AIR-SOFC" into pure oxygen "O_2" directed to the anode unit. This pure O_2 stream is labeled “TO-ANODE” with a flow rate given in Tab.2. The remaining air flow rate is labeled as "C-OFF" exiting the cathode unit. At high temperatures, pure oxygen (O_2) is introduced to the cathode unit of the SOFC module, where it undergoes an electrochemical reaction with the fuel supplied from the “ANODE” side, referred to as "FEED". The "ANODE” unit is characterized by the equilibrium reactor module RGibbs. Anodic reactions (R8-R12) are given in Tab.4.

Table 4: Chemical reactions of the burner module and anode unit

Reaction		Reaction name	ΔrH_{287}
Chemical reactions specified in the Anode unit			
R8	$H_2 + ½\ O_2 \rightarrow H_2O$	Hydrogen Oxidation	+241 kJ.mol^{-1}
R9	$CH_4 + H_2O \rightarrow 3H_2 + CO$	Steam Reforming	+206 kJ.mol^{-1}
R10	$CO + H_2O \rightarrow H_2 + CO_2$	Water-Gas Shift reaction	-41 kJ.mol^{-1}
R11	$H_2 + CO_2 \rightarrow H_2O + CO$	Reverse water-gas shift reaction	+41 kJ.mol^{-1}
R12	$H_2O \rightarrow H_2 + ½\ O_2$	water electrolysis	-241 kJ.mol^{-1}
Chemical reactions specified in the Burner module			
R13	$H_2 + ½\ O_2 \rightarrow H_2O$	Hydrogen Oxidation	+241 kJ.mol^{-1}
R14	$CO + ½\ O_2 \rightarrow CO_2$	carbon monoxide oxidation	+283 kJ.mol^{-1}

The exhaust gases from the SOFC anode, labeled "A-OFF," are then directed to the burner, where they are combined with the cathodic exhaust gases, denoted as "C-OFF-1." It is crucial to maintain closely matched temperatures for the anode and cathode exhaust gases to prevent the formation of high-temperature gradients that could potentially damage the SOFC. To ensure this temperature uniformity, an additional heating module named "HEATER-1" is employed to simulate the thermal exchange process. The appropriate amount of heat to be supplied to the flow is calculated using the TRANSFERT T-2 function.

In short, the syngas generated in the reformer, along with the oxidant, is directed into the SOFC module via the "CATHODE," "ANODE," and "HEATER-1"units, where an electrochemical reaction occurs to generate the required electrical power. After the electrochemical and chemical internal reforming reactions that take place within the SOFC module, the remaining exhaust gases are directed to a burner for combustion. The temperature of the exhaust gases is calculated using the ASPEN PLUS Design-Specs DS-1 function. To simulate the combustion process under adiabatic conditions, we employed the ASPEN PLUS RStoic reactor module named 'BURNER.' Only H_2 and CO gases remaining in the anode exhaust (A-OFF) react with oxygen in the cathode exhaust (C-OFF-1), assuming complete conversion. The chemical combustion reactions specified in the burner module (R13 and R14) are given in Tab.4.
Finally, it is assumed that the heat losses generated by the small level SOFC system are split equally (each of 7 [W]) and are represented by the heat loss: “S2” from the reformer and “S1” from the burner and “Q1” from the anode, respectively.

3. Electrochemistry module

As mentioned earlier, in the kinetic model the transfer of ions in the SOFC module cannot be effectively modeled within ASPEN PLUS (Doherty et al., 2010). In contrast, MATLAB, a powerful programming software, is well-suited for ion transfer modeling due to its advanced capabilities in mathematical evaluation, solving complex equations, and yielding detailed performance curves and power output data. Therefore, for this section an electrochemical model is developed using MATLAB software in order to evaluate the fuel cell polarizations, electrical output and select the optimum way for electricity production using a small level flared gas-fuel SOFC system.

.1. Open Circuit Voltage

Losses in a module of SOFC are directly related to the complexity of the electrochemical chemistry at the electrode-electrolyte interface, as well as to the intrinsic electrical resistance of the cell components, and are classically categorized into activation losses, ohmic losses and concentration losses, while directly influencing the cell voltage, a key indicator of its energy efficiency.
The actual voltage was calculated from Eq. (1):

$$V = V_N - V_{Act} - V_{Ohm} - V_{Conc} \quad (1)$$

Where: V_N is the Nernst voltage equation, V_{Act} is the activation loss, V_{Ohm} is the Ohmic voltage loss, and V_{Conc} is the concentration loss.
The reversible Nernst voltage, V_N, was determined from Eq. (2):

$$V_N = E_0 + \frac{RT}{2F} ln(\frac{P_{H_2} P_{O_2}^{0.5}}{P_{H_2O}}) \quad (2)$$

where: E_0 is the reversible potential [J . mol^{-1}] at standard conditions of 1 [bar], *2* represents the number of electrons produced per mole of hydrogen fuel reacted, *F* is the Faraday constant, *F = 96 485* [C . mol^{-1}], T is the average SOFC temperature [K], *R* is the molar gas constant, *R = 8.314* [J . mol^{-1}K^{-1}], P_i is the partial pressure of gaseous i [bar].
The reversible potential, E_0 , was determined from Eq. (3)**Error! Reference source not found.** (Pianko-Oprych & Palus, 2017) :

$$E_0 = \frac{4187.(58{,}3-(0{,}0113+9{,}6.10^{-7}.T).T)}{2F} \quad (3)$$

3.2. Activation voltage loss

Activation polarization predominates at low current density (*j*), where reactant species must overcome an energy barrier known as activation energy to drive the electrochemical reaction responsible for electron transfer at the solid electrolyte interfaces throughout the cell. The Butler-Volmer equation accurately describes activation polarization as follows, Eq. (4):

$$V_{Act} = \left(\frac{RT}{n\beta_{anode}F}\right) ln\left(\frac{j}{j_{0,anode}}\right) - \left(\frac{RT}{n\beta_{cathode}F}\right) ln\left(\frac{j}{j_{0,cathode}}\right) \quad (4)$$

Where: β is the conversion energy coefficient into electrical one, *j* the current density given in Eq. (5) , and j_0 is the exchange current density taken from (Pianko-Oprych & Palus, 2017) :

$$j = \frac{i_{cell}}{A_{cell}} \quad (5)$$

Where : i_{cell} the current flowing through the SOFC [A], and A_{cell} is the surface area of the SOFC [m^2].

3.3. Ohmic voltage loss

At medium current levels, ohmic losses appear(s). These losses are mainly due to the resistance of materials i.e., electrodes and current collectors to the flow of electrons and the

resistance of electrolyte to the flow of ions passing through it (Mejdoub et al., 2019). It obeys to Ohm's law and is expressed by Eq. (6):

$$V_{Ohm} = i_{cell} \times R_{Ohm} \quad (6)$$

Where, i_{cell} is the current flowing through the unit cell, and R_{Ohm} is the total unit cell resistance, which includes electronic, ionic and contact resistances, the necessary equations to calculate R_{Ohm}, were taken from (Pianko-Oprych & Palus, 2017).

3.4. Concentration loss

Concentration losses within the SOFC electrodes have an obvious impact on the performance of the cell at high current density. Those losses evaluate the resistance of the porous electrode structure to the transport of reactants approaching the reaction sites, and to the transport of products leaving the reaction sites. This is measured as a function of the concentration difference of gas species between the electrode surface (C_k^B) and the electrode-electrolyte interface (C_k^S) (Elleuch et al., 2012), and is defined using Fick's law as follows:
The concentration overpotential is defined using the Fick's law eq. (7):

$$V_{Conc} = \frac{RT}{nF} \sum ln(1 - \frac{j}{j_{lim,k}}) \quad (7)$$

Where: $j_{lim,k}$ is the current density at the anode and cathode sides, which can be obtained with maximum fuel consumption during the reaction, given by the following Eq. (8):

$$j_{lim,k} = nFD_{effi} (\frac{C_i^B}{\delta_k}) \quad (8)$$

The bulk concentration C_i^B is determined using Henry's law: $C_i^B = K_i \times P_i$, where K_i is the solubility for dissolved gases i obtained from (Elleuch et al., 2012). P_i is the partial pressure of gases i (H_2 and O_2). Values of the partial pressure of these gases are determined by ASPEN PLUS software. D_{effi} is the effective gas diffusion factor that is employed to account for the tortuous path of the molecules in the porous electrodes. By using the parallel pore model, the effective diffusion factor can be calculated by the binary diffusion coefficient of H_2 into a H_2–H_2O mixture, and O_2 into an O_2–N_2 mixture (Pianko-Oprych & Palus, 2017).
Based on the expected power, the rest of the process parameters such as hydrogen and oxygen flow rates, voltage and current density are determined.

3.5. Model interaction process

Fig. 3 depicts the operational sequence, demonstrating that the outputs extracted from the ASPEN PLUS software were used as inputs to the MATLAB software. This data transfer provided detailed information on system performance, establishing an interconnection between the two specialized software platforms.

Figure 3: Flowchart of the small level flared gas-fuel SOFC model

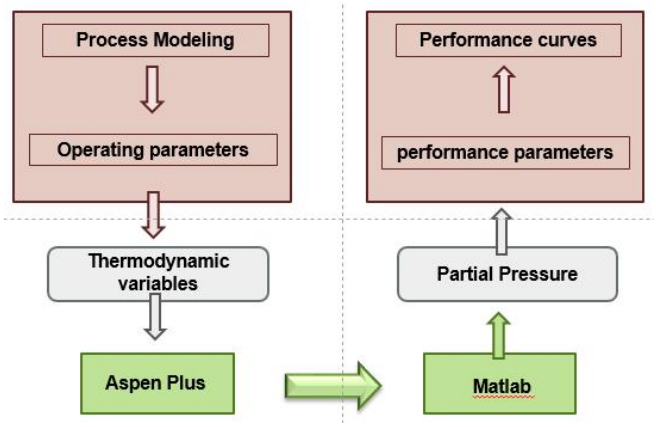

The results extracted from all branches of the ASPEN software are comprehensively reported in Tab.5.

Table 5: Quantitative results in the Partial oxidation (PO) Scenario

Stream no.	T [°C]	P [Bar]	Flow Rate [Kmol.h^{-1}]	Gas Composition						
				H_2	CH_4	H_2O	CO	CO_2	O_2	N_2
CH4	20	1.035	0.00120139	0	1	0	0	0	0	0
AIR	20	1.035	0.00348995	0	0	0	0	0	0.21	0.79
FEED	665	1.035	0.00604596	0.308014	0.0260765	0.0372523	0.140093	0.0325403	0	0.456024
TO-ANODE	635	1.035	0.00153219	0	0	0	0	0	0.924729	0.075271
A-OFF	845	1.035	0.0064766	0.0511726	2.57029e-8	0.319821	0.0269754	0.158522	0	0.443509

The operating parameters required for the electrochemical model are listed in Tab.6.

Table 6: Model input parameters

Geometry parameters	
Active fuel cell surface [m^2]	0.00163
Anode thickness [m]	0.00056
Cathode thickness [m]	0.000033
Electrolyte thickness [m]	0.00001
Interconnection thickness [m]	0.0017
Material properties	
Specific resistivity of anode [Ω.m]	ρ_{anode} = 2.98 10-5 exp ($\frac{-1392}{T}$)
Specific resistivity of cathode [Ω.m]	ρ_{anode} = 8.114 10-5 exp ($\frac{600}{T}$)
Specific resistivity of electrolyte [Ω.m]	ρ_{anode} = 2.94 10-5 exp ($\frac{10350}{T}$)
Specific resistivity of interconnection [Ω.m]	ρ_{anode} = 1.2568 10-3 exp ($\frac{4690}{T}$)
Activation polarization	
Activation energy of anode [$J.mol^{-1}$]	11000
Activation energy of cathode [$J.mol^{-1}$]	120000
Diffusion polarization	
Electrode porosity [-]	0.35
Electrode torturosity [-]	3.8
Pre-exponential factor	
Anode [$A.m^{-2}$]	2.09 109
Cathode [$A.m^{-2}$]	5.19 108

4. Results and discussion

4.1. Model validation

Given that ASPEN PLUS is a software specializing in chemical calculations, it cannot directly calculate parameters such as the current, voltage, and output power of the small level flared gas-fuel SOFC. Notably, the correctness of the SOFC model in terms of current–voltage–power model is directly related to the correctness of the simulation results. For this reason, this study compared its results with the results of other studies for verification. Fig.4(a) and 4(b) provide a comparison of the small level flared-gas SOFC model under the first reforming scenario (OP), in this study with the results in the literature (Pianko-Oprych & Palus, 2017). The curves in the figure overlap well, which verifies the reliability of the SOFC model in this study. The average absolute deviation (AAD) between our simulated results model and experimental data in the literature is about 5.59% in terms of voltage (Fig.4a) and 6% in terms of power (Fig.4b). In the linear range (Fig.4a) where ohmic losses dominate, a very satisfactory

agreement is observed. However, a slight deviation appears in the region of high current density, from 5000 A·m^{-2}.

This zone is particularly sensitive to concentration losses. It seems that the reproduction of species diffusion phenomena is more complex compared to the experiment, leading to a slight increase in concentration losses and, consequently, this slight AAD. Since the power density curve delivered by the cell as a function of current density is directly linked to the previous curve Fig.4(b), the same behavior was considered. Very good agreement in areas of low and medium current densities, while a slight deviation from 5000 A. m^{-2}. The maximum power delivered by the SOFC elementary cell with internal methane reforming by partial oxidation in our model is approximately 2431 W.m^{-2}.

Figure 4: Comparison of polarization curves (a) I–V, (b) I–P, (•) with experimental data from literature, (▪). In case of the partial Oxidation scenario.

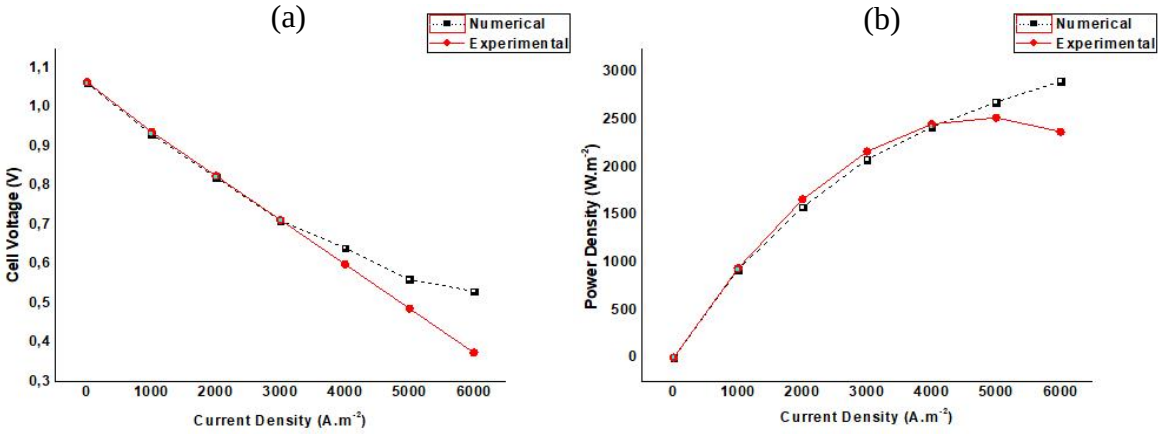

4.2. An In-Depth Comparative Analysis of Three Distinct Reforming Scenarios of the small level flared gas-fuel SOFC model

Fig.5. represents a comparison between the 3 scenarios: PO, SR and DR. Data analysis conclusively demonstrates that steam reforming stands out as the most efficient method in terms of power Fig5.a and electrical current generated Fig 5.b. This observation suggests that steam reforming has notable advantages over the other processes examined. When reactions in the reformer reactor are changed, it results in changes in the output of the reforming streams and, therefore, in most reactors. The composition of the gases at the outlet of each block of the model is presented in Tab.7. The main difference appears at the outlet of the reforming reactor ”FEED” as well as at the anode reactor ”A-OFF”.

Table 7: Quantitative results in Steam Reforming (SR) Scenario

Stream no.	T [°C]	P [Bar]	Flow Rate [Kmol.h^{-1}]	Gas Composition						
				H_2	CH_4	H_2O	CO	CO_2	O_2	N_2
CH_4	20	1.035	0.00120139	0	1	0	0	0	0	0
H_2O	20	1.035	0.000732848	0	0	1	0	0	0	0
FEED	665	1.035	0.00306381	0.572 552	0.207 782	0.035 3248	0.164 812	0.019 529	0	0
TO-ANODE	635	1.035	0.00153219	0	0	0	0	0	0.924 729	0.075 271
A-OFF	845	1.035	0.00445214	0.317 161	2.354 78e-5	0.387 089	0.125 64	0.144 182	0	0.025 9044

Fig.5. highlights that the short-circuit voltage generated by the SOFC cell in the case where there is internal SR is higher than that of the other two experiments. We reach an OCV (Open Circuit Voltage) of around 1.209 V, compared to 1.026 V and 1.037 V for PO and DR respectively. This voltage difference can be explained by several factors. First, SR, by producing hydrogen-rich syngas, provides purer and higher-quality fuel for the SOFC fuel cell. The content of H_2 produced and diffusing towards the anodic reaction zone is higher in the case of SR (yH_2= 0.5725) compared to that of PO (yH_2= 0.308) and DR (yH_2= 0.347) as illustrated in Tab.7. Additionally, SR can enable better use of the energy contained in the fuel, as it is an efficient conversion process that optimizes H_2 production.

Figure 5: Comparison of simulation results based on three scenarios including (—•—) SR steam reforming, (- - -) PO partial oxidation, (—▶—) DR dry reforming in term of (a) I–V and (b) I–P curves of SOFC.

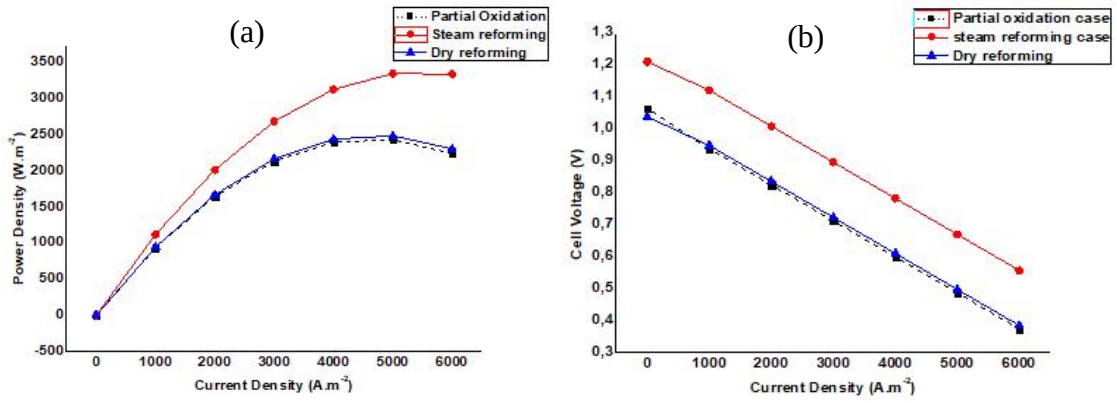

While, in the case of DR the results are very close to those of PO, which can be explained by the fact that both reactions produce almost similar amounts of H_2. In contrast, the latter two experiments could have energy losses due to side reactions or a less optimal fuel supply, which could result in a lower OCV.

While methane can be employed as a fuel source in SOFCs, electro-kinetic factors related to specific consumption concerns indicate a sluggish reaction rate. This underscores the importance of sustaining a substantial quantity of hydrogen in the anode, which must be generated through SR and shifting reactions (Damo et al., 2019). The improvement obtained in the SR scenario is also visualized on the power curve of the SOFC cell. It is that the internal methane steam reforming was more efficient. The maximum power reached is of the order of 3347.6 Wm^{-2} while that of PO and DR does not exceed 2431 Wm^{-2} and 2485.5 Wm^{-2} respectively. This result seems reasonable due to the use of a high quality hydrogen-rich synthesis gas, which makes it possible to improve the efficiency of the electrochemical reaction in the fuel cell and increase electricity production. Taking into account the reactive surface area of the cell (0.00163 m^2), the cell delivers a power of 5.456 W, 3.962 W and 4.051 W in the case of internal SR, partial methane oxidation and DR respectively.

4.3. Performance analysis of the small level flared gas-fuel SOFC system powered by real composition flared gas

When simulating the SOFC with flared gas real composition, a significant decrease in performance was observed (Fig.6) which can be attributed to several factors. When the gas composition was altered, the amount of CH_4 was reduced from 100% to 81%. This reduction has directly impacted the production of H_2, because methane is the main precursor for its generation at the anode following the methane steam reforming reaction. Since hydrogen is the fuel that could react electrochemically in the SOFC anodic reaction sites, a reduction in its quantity induced a consequent drop in electrical energy production. This reduction is manifested by a reduction in the cell voltage and final power output. The results obtained thus confirm the sensitivity of the SOFC to the composition of the feed gas, with direct implications for its performance. Previous studies, such as those conducted by (Harun et al., 2016), have also demonstrated the critical impact of gas composition on SOFC cell performance, thus strengthening the validity of our results.

Figure 6: Performance comparison of (a) I–V, (b) I–P curves of the small level SOFC when fed by methane and flared gas based on the SR scenario.

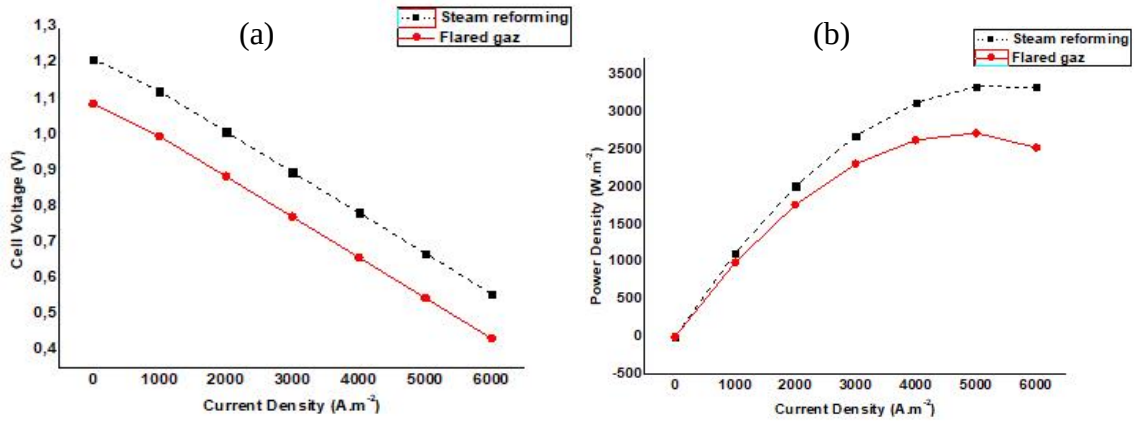

Fig.6. presents the results obtained in terms of voltages and power density, compared with the case of SR when the cell is powered with 100% of CH_4. The maximum power reached is of the order of 2725 Wm^{-2}. Taking into account the reactive surface area of the cell (0.00163 m^2), the cell delivers a power of 4.441 W. In addition, this can be explained by the fact that reactions are favored when the stoichiometric ratio is balanced between methane, water vapor and oxygen. By decreasing the amount of methane, the stoichiometric ratio is unbalanced, which reduces the efficiency of the steam reforming reaction and consequently, the cell voltage decreases. The gas composition results in each stream are detailed in the Tab.8.

Table 8: Gas composition for the outlet stream in the small level flared gas-fuel SOFC system

Stream no.	T [°C]	P [Bar]	Flow Rate [Kmol.h^{-1}]	Gas Composition						
				H_2	CH_4	H_2O	CO	CO_2	O_2	N_2
Flared gas (a)	20	1.035	0.00120139	0	0.8194	0	0	0.0072	0	0.0129
H2O	20	1.035	0.000600496	0	0	1	0	0	0	0
FEED	665	1.035	0.00288926	0.457062	0.333254	0.0124021	0.182412	0.0095057	0	0.0053639
TO-ANODE	635	1.035	0.00153219	0	0	0	0	0	0.924729	0.075271
A-OFF	845	1.035	0.00492936	0.394137	9.57461e-5	0.271502	0.186753	0.120971	1.941 2e-18	0.0265405

(a) To the gas composition: add → C_2H_6=0.0776, C_3H_8=0.0566, i-C_4H_{10}=0.0061, n- C_4H_{10}=0.0149, i-C_5H_{12}=0.0024, nC_5H_{12}=0.0019, 22-MPropane (C_5H_{12})=0.0001, C_6H_6=0.0009.

4.4. Potential applications of the Small level flared gas-fuel SOFC system

The studied small scale SOFC can respond to a wide spectrum of small electricity production applications. It can power lightweight electronic devices, or other small device charging stations for cell phones, tablets or small electronic devices. It is noteworthy to note that SOFCs are among the good options for clean, efficient, and economical energy production, for small standalone applications in remote areas and especially when fuel for SOFC is available such as in the case of flared gas generally recuperated from gas & oil industries installed in isolated areas.

On the other hand, the stationary energy sector includes a diverse range of applications, such as micro-grids, cogeneration systems, residential as well as industrial facilities, which are required applications for the oil & gas industries. In fact, in order to expand the SOFC application to meet the growing energy needs of this type of industry, the SOFC system should be upscaled to reach kW-level applications. This involves combining multiple single cells in series and in parallel to form a complete stack. Furthermore, the integration of a gas turbine into the SOFC stack have demonstrated the ability to enhance the overall system efficiency, enabling the system to attain power levels in the kilowatt range (Al-Khori et al., 2020 ; Sghaier et al., 2018).

5. Conclusion

In conclusion, this modeling work using ASPEN PLUS and MATLAB software made it possible to define a trend approach for the valuation of flared gas, a source of major concern due to its harmful effects on the environment and all beings alive. The simulations began by studying three SOFC cell scenarios (PO, SR and DR) powered by different gas composition, highlighting that the mixture of 100% methane (CH_4) with steam (H_2O) offers the highest power and is therefore chosen as the base model. The second step consisted of introducing a real flared gas compositions into the model, showing that even when the proportion of CH_4 is less than 100%, the power delivered has decreased but remains satisfactory. In addition, it was clear that heavy hydrocarbons are also suitable for supplying SOFC, which opens interesting perspectives for the valorization of other types of fuel, such as the studies carried out by Elleuch et al., who have proven in their works the possibility of powering fuel cells with bio-oils and even solid bio-char resulting from the carbonization of biomass. The next step of our work is to further improve our model to make it suitable on an industrial scale of oil & gas inductries. By integrating a gas turbine, we aim to achieve a kW level flared gas-fuel TG-SOFC system.

References

Al-Khori, K., Bicer, Y., & Koc, M. (2020). Integration of Solid Oxide Fuel Cells into oil and gas operations: needs, opportunities, and challenges. *Journal of Cleaner Production*, *245*, 118924.

Aydin, G. (2015). The modeling and projection of primary energy consumption by the sources. *Energy Sources, Part B: Economics, Planning, and Policy*, *10*(1), 67–74.

Böttcher, K., Paunu, V.-V., Kupiainen, K., Zhizhin, M., Matveev, A., Savolahti, M., Klimont, Z., Väätäinen, S., Lamberg, H., & Karvosenoja, N. (2021). Black carbon emissions from flaring in Russia in the period 2012–2017. *Atmospheric Environment*, *254*, 118390.

Choudhury, A., Chandra, H., & Arora, A. (2013). Application of solid oxide fuel cell technology for power generation—A review. *Renewable and Sustainable Energy Reviews*, *20*, 430–442.

Damo, U. M., Ferrari, M. L., Turan, A., & Massardo, A. F. (2019). Solid oxide fuel cell hybrid system: A detailed review of an environmentally clean and efficient source of energy. *Energy*, *168*, 235–246.

Dicks, A. L., Pointon, K. D., & Siddle, A. (2000). Intrinsic reaction kinetics of methane steam reforming on a nickel/zirconia anode. *Journal of Power Sources*, *86*(1–2), 523–530.

Doherty, W., Reynolds, A., & Kennedy, D. (2010). Computer simulation of a biomass gasification-solid oxide fuel cell power system using Aspen Plus. *Energy*, *35*(12), 4545–4555.

Elleuch, A., Boussetta, A., & Halouani, K. (2012). Analytical modeling of electrochemical mechanisms in CO2 and CO/CO2 producing direct carbon fuel cell. *Journal of Electroanalytical Chemistry*, *668*, 99–106.

Elleuch, A., & Halouani, K. (2020). Intermediate-temperature solid oxide fuel cell fueled by biofuels. In *Intermediate temperature solid oxide fuel cells* (pp. 427–476). Elsevier.

Harun, N. F., Tucker, D., & Adams II, T. A. (2016). Impact of fuel composition transients on SOFC performance in gas turbine hybrid systems. *Applied Energy*, *164*, 446–461.

Höber, M., Königshofer, B., Schröttner, H., Fitzek, H., Menzler, N. H., Hochenauer, C., & Subotić, V. (2023). Experimental identification of the impact of direct internal and external methane reforming on SOFC by detailed online monitoring and supporting measurements. *Journal of Power Sources*, *581*, 233449.

Kang, Y.-W., Li, J., Cao, G.-Y., Tu, H.-Y., Li, J., & Yang, J. (2009). A reduced 1D dynamic model of a planar direct internal reforming solid oxide fuel cell for system research. *Journal of Power Sources*, *188*(1), 170–176.

Kapsalyamova, Z., & Paltsev, S. (2020). Use of natural gas and oil as a source of feedstocks. *Energy Economics*, *92*, 104984.

Khalili-Garakani, A., Iravaninia, M., & Nezhadfard, M. (2021). A review on the potentials of flare gas recovery applications in Iran. *Journal of Cleaner Production*, *279*, 123345.

Khalili-Garakani, A., Nezhadfard, M., & Iravaninia, M. (2022). Enviro-economic investigation of various flare gas recovery and utilization technologies in upstream and downstream of oil and gas industries. *Journal of Cleaner Production*, *346*, 131218.

Loe, J. S. P., & Ladehaug, O. (2012). Reducing gas flaring in Russia: Gloomy outlook in times of economic insecurity. *Energy Policy*, *50*, 507–517.

Mejdoub, F., Elleuch, A., & Halouani, K. (2019). Assessment of the intricate nickel-based anodic reactions mechanism within a methanol fed solid oxide fuel cell based on a co-ionic conducting composite electrolyte. *Journal of Power Sources*, *414*, 115–128.

Nezhadfard, M., & Khalili-Garakani, A. (2020). Power generation as a useful option for flare gas recovery: Enviro-economic evaluation of different scenarios. *Energy*, *204*, 117940.

Pianko-Oprych, P., & Palus, M. (2017). Simulation of SOFCs based power generation system using Aspen. *Polish Journal of Chemical Technology*, *19*(4), 8–15.

Saidi, M., Siavashi, F., & Rahimpour, M. R. (2014). Application of solid oxide fuel cell for flare gas recovery as a new approach; a case study for Asalouyeh gas processing plant, Iran. *Journal of Natural Gas Science and Engineering*, *17*, 13–25.

Shahab-Deljoo, M., Medi, B., Kazi, M.-K., & Jafari, M. (2023). A Techno-Economic Review of Gas Flaring in Iran and Its Human and Environmental Impacts. *Process Safety and Environmental Protection*. https://doi.org/10.1016/j.psep.2023.03.051

Tahmasebzadehbaie, M., & Sayyaadi, H. (2023). Techno-economic-reliability assessment of a combined NGL refinery and CCHP system driven by wasted energy of flare and flue gases. *Process Safety and Environmental Protection*, *171*, 152–166.

Tan, L., Dong, X., Chen, C., Gong, Z., & Wang, M. (2021). Diverse system layouts promising fine performance demonstration: A comprehensive review on present designs of SOFC-based energy systems for building applications. *Energy Conversion and Management*, *245*, 114539.

Zhang, C., Wang, J., Li, L., & Gang, W. (2019). Dynamic thermal performance and parametric analysis of a heat recovery building envelope based on air-permeable porous materials. *Energy*, *189*, 116361.